Geomechanics and Engineering, *Vol. 31, No. 1 (2022) 1-14*
https://doi.org/10.12989/gae.2022.31.1.001

Influence characteristics of isolation piles on deformation of existing shallow foundation buildings under deep excavation

Xinrong Liu[1], Peng Liu[1], Xiaohan Zhou[*1], Linfeng Wang[**1], Zuliang Zhong[1], Xihui Lou[2], Tao Chen[2] and Jilu Zhang[1]

[1]*College of Civil Engineering, Chongqing University, Chongqing 400045, China*
[2]*China Railway Major Bridge Reconnaissance & Design Institute Co., Ltd., Wuhan Hubei 430050, China*

(*Received June 3, 2021, Revised June 24, 2022, Accepted July 23, 2022*)

Abstract. Urban deep excavation will affect greatly on the deformation of adjacent existing buildings, especially those with shallow foundations. Isolation piles has been widely used in engineering to control the deformation of buildings adjacent to the excavation, but its applicability is still controversial. Based on a typical engineering, numerical calculation models were established and verified through monitoring data to study the influence characteristics of isolation piles on the deformation of existing shallow foundation buildings. Results reveal that adjacent buildings will increase building settlement δ_v and the deformation of diaphragm walls δ_h, while the isolation piles can effectively decrease these. The surface settlement curve is changed from "groove" type to "double groove" type. Sufficiently long isolation pile can effectively decrease δ_v, while short isolation piles will lead to a negative effect. When the building is within the range of the maximum settlement location P, maximum building rotation θ_m will increase with the pile length L and the relative position between isolation pile and building d/D increase (d is the distance between piles and diaphragm walls, D is the distance between buildings and diaphragm walls), instead, θ_m will decrease for buildings outside the location P, and the optimum was obtained when d/D=0.7.

Keywords: deep excavation; deformation characteristics; existing buildings; isolation pile; numerical simulation

1. Introduction

Construction of urban rail transit contributed to an economic boom, but the deep excavation of the metro station will cause varying degrees of impact on the surrounding structures (Mansouri and Asghari-Kaljahi 2019, Mitew-Czajewska 2018, Jiang *et al*. 2018, Qian *et al*. 2020). The damage of adjacent buildings caused by excavation is mostly due to the lack of soil bearing capacity or excessive deformation of supporting structures, resulting in excessive surface subsidence outside the excavation. Therefore, appropriate steps must be taken to control structures deformation and keep it within safe limits. However, the influence of excavation on adjacent buildings is closely related to geological conditions, excavation methods (Talha 2001), relative position of building and the excavation (Castaldo *et al*. 2013, Maddah *et al*. 2021), structure forms (Son and Cording 2005, Zhandos *et al*. 2015), construction procedures and geometry of the excavation (Yang *et al*. 2019).

Controlling measures of deformation of adjacent buildings during excavation has been investigated extensively in recent years. Some concentrated on the perspective of controlling the deformation of the retaining structures to reduce the impact on the building. Studies shows a trend for decreasing wall displacement with increasing system stiffness (Rezvani and Tutunchian 2021), Wang *et al.* (2010) investigated that horizontal displacement resulted by supporting structures with high stiffness (including diaphragm walls, the lateral displacements of walls of diaphragm walls, contiguous pile walls) is obviously smaller than that resulted by supporting structures with smaller stiffness (including sheet pile walls, compound soil nail walls, deep soil mixing walls). Chen *et al*. (2015), Li *et al*. (2014) proposed a novel construction method DAEM and channel-type excavation scheme respectively. Chen *et al*. (2016), Chowdhury *et al*. (2013), Wang *et al*. (2010) put forward optimization on the excavation measures and supporting schemes. Some studies focused on the improvement of the bearing capacity of the corresponding soil near the structures. Ou *et al*. (2008) analyzed the characteristics of partial ground improvement by jet grouting or mechanical deep mixing method. Zhang *et al*. (2020) investigated the effects of a ground improvement method of jet grout piles on the excavation performances. In addition, apply isolation piles is another method of reducing the soil deformation and was frequently used in practice, which can halt the propagation of soil deformation and stress effectively due to excavation (Nikiforova and Vnukov 2012). Excavation will break through the original stress state of the structures and soils, and isolation piles can hinder stress path of soil outside excavation, which is helpful to reduce soil deformation around the excavation and protect existing structures.

Most of the existing research about isolation piles was

*Corresponding author, Ph.D.
E-mail: zhouxh2008@126.com
**Corresponding author, Ph.D.
E-mail: 476964211@qq.com

ISSN: 2005-307X (Print), 2092-6219 (Online)

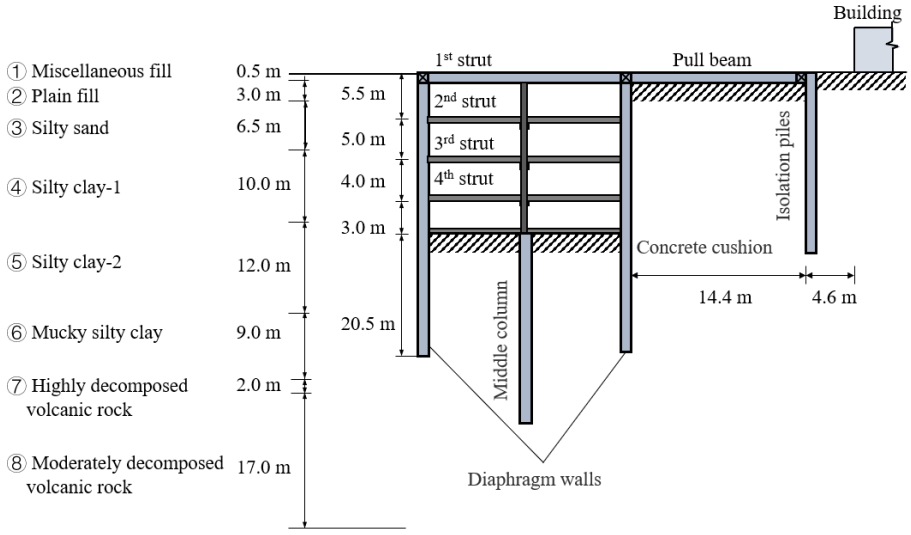

Fig. 1 Deep excavation layout

concentrated on the mechanisms of decreasing the soil deformation and controlling the deformation of the existing buildings due to excavation (Zheng *et al*. 2018, Gao *et al*. 2006). Demeijer *et al*. (2018) carried out numerical simulation to demonstrate the effectiveness of isolation piles and revealed that isolation piles can indeed reduce the deformation of the diaphragm walls, earth pressure, and soil movement. Yao *et al*. (2012) made comparison between the construction conditions using isolated piles and those without isolation piles, and verified the positive role of the isolation piles. In addition, the influence of pile diameter (Kumara *et al*. 2016), pile length (Shen *et al*. 2017), pile spacing (Bilotta and Russo 2011), the roughness of its interface (Bilotta 2008, Canakci and Hamed 2017), and spatial position on controlling structure deformation were also researched to deepen the understanding of isolation piles.

Existing studies mainly concentrated on the deformation control of the adjacent structures due to excavations, but few paid attentions to the reinforcement mechanism of isolation piles. In addition, though isolation piles have been widely applied to protecting adjacent buildings near the excavation and achieved positive results (Yao *et al*. 2012, Cui *et al*. 2016), but more remarkable cases showed that some projects with isolation piles reflected a negative effect (Zheng *et al*. 2018). It is necessary to do more research to obtain reasonable practical design recommendations and understand the working mechanisms of the isolation piles.

Nanjing Hotel is only 20 meters away from the deep excavation of Hongqiao Subway Station in Nanjing, China, and the foundation style is shallow foundation, which will suffer more serious deformation problems and threat the safety of heritage buildings (Tan *et al*. 2016). Besides, as a cultural relics architecture, it has stricter deformation control requirement. To control deformation of Nanjing Hotel, a row of isolation piles was set up in advance before excavation. By taking the excavation of Nanjing Hongqiao Subway Station in China as the background, the numerical modeling of the excavation was established to study the effect of the isolation piles on adjacent buildings with shallow foundation. By comparing the different working conditions with and without isolation piles, building settlement δv and building rotation θ were used as the measurement indexes of building damage. Influence characteristics of isolation piles on deformation of existing shallow foundation buildings were analyzed. In addition, in order to further understand the supporting effect of isolation piles on buildings in different locations outside the excavation, a large number of parametric studies were carried out to study the influence of the relative position of excavation-pile-building and the isolation pile length. Finally, three typical types were concluded according to different building positions and the corresponding supporting effect. The results are helpful for designing protective and economic measures in the real project.

2. Project background

2.1 Project description

The location for the investigated deep excavation for the Hongqiao Station of Subway Line 5 is the Gulou Area of Nanjing. Fig. 1 presents the site plan for the project, and is arranged along Zhongshan North Road. The investigated deep excavation is located on the north side of the intersection of Zhongshan North Road and Xinmofan Road. The length of the excavation is 219.00 m long, the width and depth of the standard section is 18.5m and 18.76m, respectively, with about 2.79 m depth soil above the roof. The width and depth of the end wells is 22.5 m and 19.9m, respectively, with 3.3 m depth soil above the roof. The station is constructed by top-down method, while semi-covered method is used at the end well to relieve the traffic.

An 800 mm thick diaphragm wall was used to support the foundation pit, and the penetration depths in the standard section and the end well were 18.50 m and 24.70 m, respectively. The bottom of the diaphragm walls of the standard section was in mucky silty clay, and that of the end well was in moderately decomposed volcanic rock. The

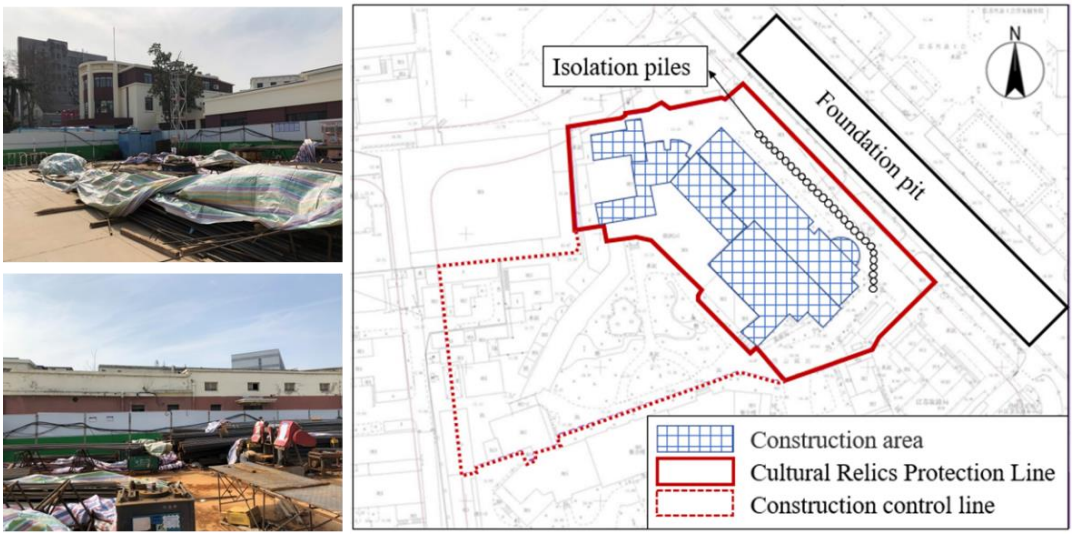

Fig. 2 Location of the excavation and the protected buildings (the building on the photos is Nanjing Hotel and isolation piles are behind the fence)

Table 1 Physical and mechanical parameters of the soil

Layer	Soil	Average thickness	Density	Cohesion	Friction angle	Lateral pressure coefficient	Elastic modulus	Poisson's ratio
		m	γ kN/m^3	c kPa	φ°	K_0	E MPa	λ
①	Miscellaneous fill	0.5	18.5	5.0	25.0	0.50	2.0	0.15
②	Plain fill	3.0	18.2	10.0	10.0	0.60	4.0	0.18
③	Silty sand	6.5	19.2	6.2	32.1	0.45	15.0	0.31
④	Silty clay-1	10.0	18.2	14.4	17.0	0.65	6.0	0.39
⑤	Silty clay-2	12.0	18.8	21.5	19.3	0.62	7.1	0.36
⑥	Mucky silty clay	9.0	20.0	35.5	15.6	0.44	12.0	0.30
⑦	Highly decomposed volcanic rock	2.0	24.0	100.0	33.0	0.30	130.0	0.23
⑧	Moderately decomposed volcanic rock	-	25.3	300.0	36.0	0.22	15000.0	0.19

excavation profile of the standard section is shown in Fig. 12, the designed supporting schemes consisted of four struts, placed 0.0 m, 5.5 m, 10.0 m, and 14.5 m below the ground surface, respectively. The 1st struts were concrete struts with 9 m horizontal space along the longitudinal direction, and the cross sections were 1.0×1.2 m. The 2nd to 4th struts were steel pipes with 4.5 m horizontal space. The cross section of the 2nd and 4th struts had an external diameter of 609 mm and a thickness of 16 mm, and those of the 3rd struts had an external diameter of 800 mm and a thickness of 16 mm. The 2nd to 4th struts were preloaded with 750 kN, 1150 kN and 600 kN, respectively. Long-term phreatic water level was at -1.2 to -2.5 m.

2.2 Ground condition

The foundation pit is located in the floodplain area of the Qinhuai River. The stratigraphic profile can be seen in Fig. 12, the physical and mechanical parameters of the soils and rocks are referred to the Geological survey report and shown in Table 1.

The excavation is located in a saturated weak pervious layer, with the ground water level is 0.80 m-2.70 m, and an annual variation of about 1.0 m. The permeable layer is mainly consisting of filled soil, silty sand and gravel layer, while the rest of the stratum is relatively impermeable layer.

2.3 Isolation piles and building condition

Nanjing Hotel is a two-storey brick and concrete structure with shallow foundation. In 1992, Nanjing Hotel was listed as the cultural relics protection architecture of Nanjing, and subsequently in 2002 as the cultural relics protection architecture of Jiangsu Province. The environmental risk level of the excavation is level II, and the control value of the building settlement is 10-30 mm. The location of Nanjing Hotel and the excavation is shown in Fig. 2.

Foundation type is an important factor to building deformation. In general, pile foundation is stronger than shallow foundation in resisting building deformation caused by excavation (Tan *et al*. 2010). Therefore, deformation of adjacent buildings with shallow foundation will be more serious due to excavation. To protect Nanjing Hotel, isolation piles with a diameter of 1.0 m, a spacing of 1.2 m and a length of 21.1 m were constructed to control building deformation. The distance between the piles and the building is 4.6 m and the bottom of the piles is located in

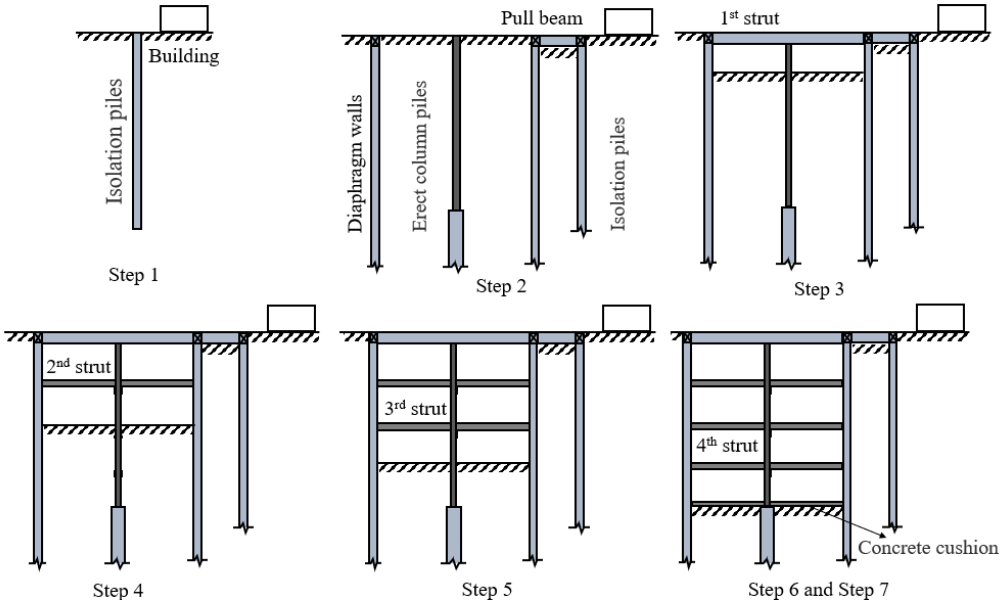

Fig. 3 Construction procedure

silty clay-2.

2.4 Construction procedure

The station excavation was constructed by top-down method. The construction process of the excavation was listed below and was shown in Fig. 3, and tube well dewatering is used with open ditch drainage.

- *Step 1*: construct the isolation piles;
- *Step 2*: construct diaphragm walls, erect column piles, and pull beams;
- *Step 3*: install 1st concrete strut and excavate 1st floor soils;
- *Step 4*: install 2nd steel strut and excavate 2nd floor soils;
- *Step 5*: install 3rd steel strut and excavate 3rd floor soils;
- *Step 6:* install 4th steel strut and excavate 4th floor soils;
- *Step 7*: construct the bottom plate.

3. Numerical simulation

3.1 Parameters

Numerical analyses were carried out using the 3D finite difference software Flac^{3D}5.0. In this model, silty sand, silty clay-1, silty clay-2 and mucky silty clay were modeled with Modified Cam-Clay Model, and the remaining soils and rocks were modeled with Mohr-Coulomb Model (Liu *et al*. 2019, Yang *et al*. 2020). The physical and mechanical parameters of each layer material are shown in Table 2, where M, λ, κ, v_λ are obtained by triaxial test combined with the following formula, and the rest parameters are referred to the Geological survey report.

In which, the friction constant M is the slope of the critical state line and can be calculated by the following formula

$$M = \frac{6\sin\varphi'}{3-\sin\varphi'} \tag{1}$$

Where φ' is the effective angle of internal friction.

λ and κ are the slopes of the normal consolidation curve and the rebound curve, respectively, and κ can be valued between (1/5-1/3) λ.

v_λ and p_1 are determined by the position of the normal consolidation curve. p_1 is generally assumed to be 1 kPa, then v_λ can be obtained by undrained shear strength c_u, friction constant M, λ and κ by the following formula

$$c_u = \frac{Mp_1}{2}\exp\left(\frac{\Gamma - v_{cr}}{\lambda}\right) \tag{2}$$

$$\Gamma = v_\lambda - (\lambda-\kappa)\ln(2) \tag{3}$$

where Γ is the intercept of the normal consolidation curve on v axis, v_{cr} is the particular specific volume.

The relationship between bulk modulus K, shear modulus G and elastic modulu E, Poisson's ratio λ is:

T is tensile strength. The tensile strength of soil is 0, while those of rock is 1/8-1/12 of compressive strength.

$$K = \frac{E}{3(1\text{-}2\lambda)} \tag{4}$$

$$G = \frac{E}{2(1+\lambda)} \tag{5}$$

In most existing projects, isolation piles are often constructed in a row. To simplify the numerical simulation, the isolation piles were transformed into a wall through bending stiffness equivalence (Fig. 4). Thus, each bored pile with a diameter of 1.0 m is transformed to a wall with a length of 1.2 m and a thickness of 0.8 m through formula (6).

Table 2 Parameters of rock and soil layers in numerical simulation

Layer	Soil	Average thickness	γ	M	λ	κ	ν_λ	K	G	c_u	φ	T
		m	kN/m^3	-	-	-	-	MPa	MPa	kPa	°	MPa
①	Miscellaneous fill	0.5	18.5	-	-	-	-	8.8	3.4	5.0	25.0	0.0
②	Plain fill	3.0	18.2	-	-	-	-	8.3	2.2	10.0	10.0	0.0
③	Silty sand	6.5	19.2	-	-	-	-	-	-	6.2	32.1	0.0
④	Silty clay-1	10.0	18.2	1.03	0.075	0.007	1.97	-	-	14.4	-	-
⑤	Silty clay-2	12.0	18.8	1.20	0.049	0.010	1.75	-	-	35.5	-	-
⑥	Mucky silty clay	9.0	20.0	1.14	0.080	0.006	2.03					
⑦	Highly decomposed volcanic rock	2.0	24.0	-	-	-	-	50	105.6	100.0	33.0	7.0
⑧	Moderately decomposed volcanic rock	17.0	25.3	-	-	-	-	4000	6302.5	300.0	36.0	10.0

Table 3 Parameters of support structures in numerical modeling

Supporting structure	Size	Density	Elastic modulus	Poisson's ratio
	mm	ρ kg/m^3	E GPa	μ
Underground diaphragm walls	800	2500	30	0.2
Concrete struts	800×1000	2500	30	0.2
Concrete uplift piles	φ1000	2500	30	0.2
Steel struts	φ609×16	7800	200	0.27
Steel lattice columns	500×500	7800	200	0.27
Isolation piles	800	2500	30	0.2

$$\frac{\pi D^4}{64}=\frac{bh^3}{12} \tag{6}$$

where D is the diameter of isolation piles, b is the equivalent width, and h is the equivalent thickness.

Supporting structures was calculated by elastic constitutive model. In addition to the geometric size and density, only the elastic modulus E and Poisson's ratio λ need to be provided, which are shown in Table 3. It is necessary to set contact between the soil and the underground structures to accurately reflect the interaction between the soil and the retaining structures. Flac^{3D} manual recommends that the normal stiffness K_n and tangential stiffness K_s can be 10 times the equivalent stiffness of the surrounding "hardest" adjacent area (Yu *et al*. 2018), i.e.

$$K_n=K_s=10\max\left[\frac{\left(K+\frac{4}{3}G\right)}{\Delta z_{\min}}\right] \tag{7}$$

where K is the bulk modulus of the surrounding "hardest" adjacent area, G is the shear modulus of the surrounding "hardest" adjacent area, and $\Delta z_{\min}$ is the minimum size of the connection area.

The cohesive force c and internal friction angle φ of the contact surface can be 0.5-0.8 times of the adjacent soil layer. The parameters for the final determination of the contact surface are shown in Table 4.

Table 4 Parameter of contact surface

Location	Normal stiffness	Shear stiffness	Cohesion	Friction angle
	K_n GPa/m	K_s GPa/m	c kPa	φ°
Side of the diaphragm walls	0.016	0.016	10	16
Bottom of the diaphragm walls	0.15	0.15	70	23
Side of the isolation piles	0.15	0.15	10	16
Bottom of the isolation piles	0.25	0.25	70	23

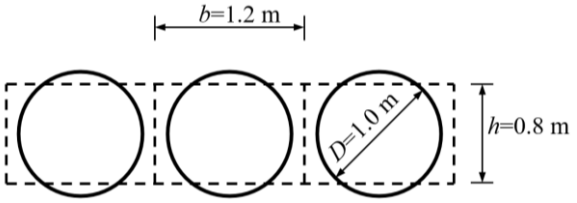

Fig. 4 Transformation of the isolation piles in simulation

3.2 Calculating model

The numerical calculation model is shown in Fig. 5, the minimum mesh size is 0.5 m, the maximum is 6.731 m, and the number of mesh is 51512. Long and narrow type of excavation is usually considered as plane strain problem, and in simulation, consider the distribution of struts (the horizontal spacing of concrete bracing and steel bracing is 9 m and 4.5 m respectively), the width of the model was decided to be 9.0 m. Considering the boundary effect of numerical simulation, model size usually extends about 3-5 times the depth of the excavation outward from the excavation edge, and the size of the building side should be enlarged appropriately. Thus, the left side of the model is 51.2 m from the pit edge and the right side is 100.0 m from the pit edge, and the total length of the model is 170.8 m. The height of the model is 60.0 m because moderately decomposed volcanic rock is 17.0 m below the basal, which can resist deformation strongly. The final size of the model is 170.8 m×9.0 m×60.0 m. The range of Nanjing Hotel was decided to be 48.0 m and was 19.0 m away from the excavation. It was considered as a two-story building with shallow foundation, and the loads of each story is 15.0 kPa.

The bottom boundary of the model was fixed totally while the top surface was left free. The lateral sides of the model were fixed in the horizontal direction while vertical movement was allowed. A concentrated force outside the

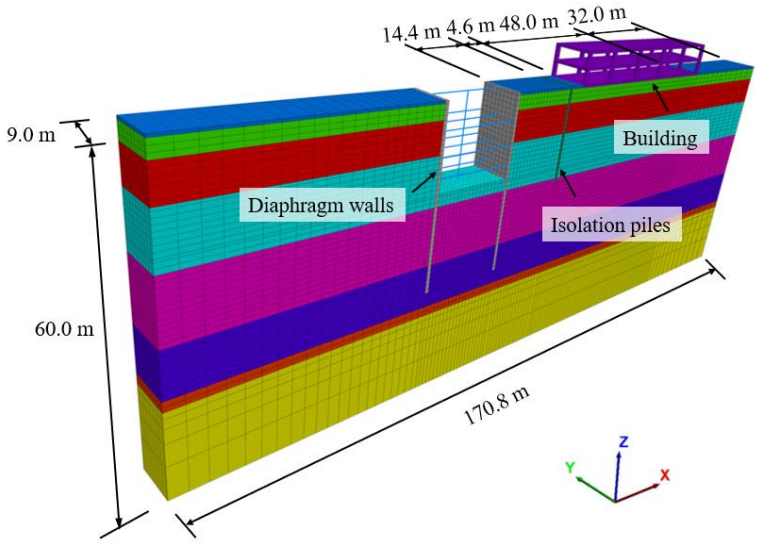

Fig. 5 Calculating model

Table 5 Numerical simulation process

Step	Procedure instructions
1	Generate an initial ground stress field
2	Reset the initial displacements to zero and construct the isolation piles, the erect column piles and diaphragm walls
3	Excavate to - 1.0 m depth
4	Install the first concrete strut
5	Dewater to - 6.0 m depth
6	Excavate to - 6.0 m depth
7	Install the first concrete strut
8	Repeat steps 3-5 until the excavation depth reaches to - 6.0 m, -11.0 m and -15.0 m respectively.

Table 6 Simulation conditions

Group	The distance between isolation piles and diaphragm walls/m	Pile length/m	Building range/m
1	16	21	20.8 - 68.8
2	No Isolation piles		20.8 - 68.8
3	16	21	No building
4	No Isolation piles		No building
5	1	30	10 - 30
6-10	3	10, 20, 30, 40, 43	10 - 30
11-15	5	10, 20, 30, 40, 43	10 - 30
16-20	7	10, 20, 30, 40, 43	10 - 30
21	9	30	10 - 30
22-26	2	10, 20, 30, 40, 43	20 - 40
27-31	6	10, 20, 30, 40, 43	20 - 40
32-36	10	10, 20, 30, 40, 43	20 - 40
37-41	14	10, 20, 30, 40, 43	20 - 40
42-46	18	10, 20, 30, 40, 43	20 - 40
47-51	3, 9, 15, 21, 27	30	30 - 50
52-56	4, 12, 20, 28, 36	30	40 - 60

excavation is applied at the joint of the steel struts and the diaphragm walls to simulate the pre-loading axial force of the steel struts, the 2nd to 4th steel struts were preloaded with 750 kN, 1150 kN and 600 kN, respectively.

3.3 Numerical simulation process

The process of numerical simulation was similar to construction procedure, and is shown in Table 5.

3.4 Simulation conditions

Table 6 shows the specific simulation conditions. The applicability of the isolation piles was verified by comparison between groups 1-4, where group 1 corresponds to the actual engineering situation. On this basis, groups 5-

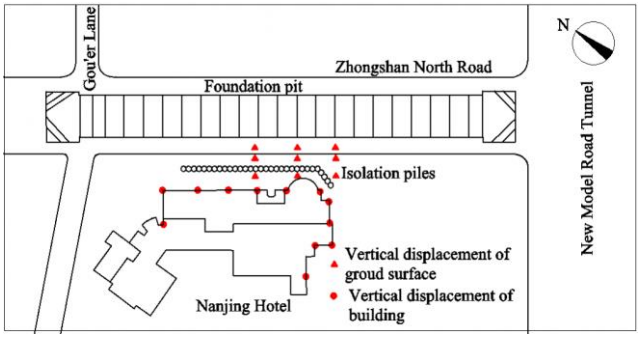

Fig. 6 Arrangement of measuring points

44 were set to study the influence of the length and location of the isolation piles on supporting effect. Then, groups 45-54 were set to study the difference of supporting effect of isolation piles on different building positions by changing the relative position of excavation-pile-building.

4. Results

4.1 Comparison with field data

In order to verify the accuracy of numerical simulation, the field data were compared with the numerical simulation results. CX-3D inclinometer (accuracy: ±0.01 mm/500 mm) was used to monitor the lateral displacement of diaphragm walls, and Trimble Dini03 electronic level (accuracy: ±0.3 mm/km) was used to monitor the vertical deformation of the building during construction. Due to the serious damage of ground settlement measuring points and building settlement measuring points, the measuring points with relatively complete preservation were selected for comparison. The arrangement of measuring points is shown in Fig. 6.

Fig. 7 shows the comparison between numerical results and field data for the lateral displacement of the diaphragm walls δ_h. The maximum lateral displacement of the diaphragm walls δ_{hm} increases continuously with the

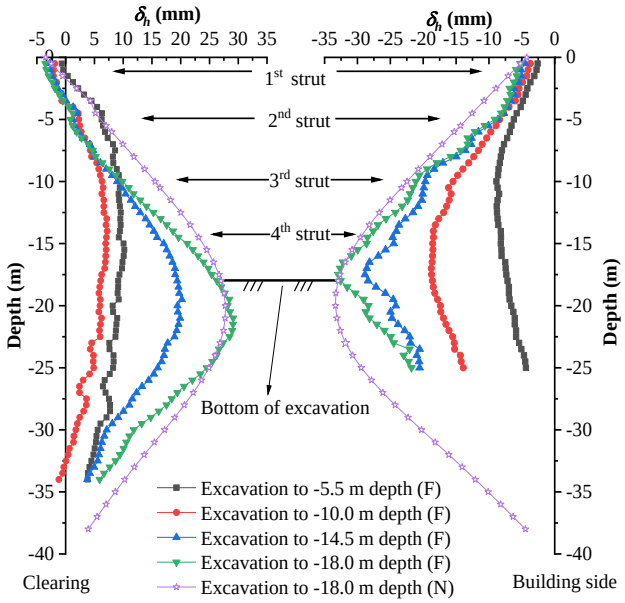

Fig. 8 Lateral displacement of diaphragm walls during excavation (F means field data; N means numerical results)

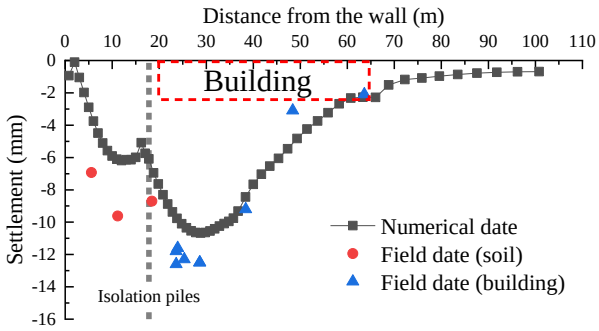

Fig. 9 Surface settlement and building settlement after excavation

excavation, and the value after the excavation is about 33.4 mm and 22.7 mm in the building side and in the clearing, respectively. The position of the maximum lateral

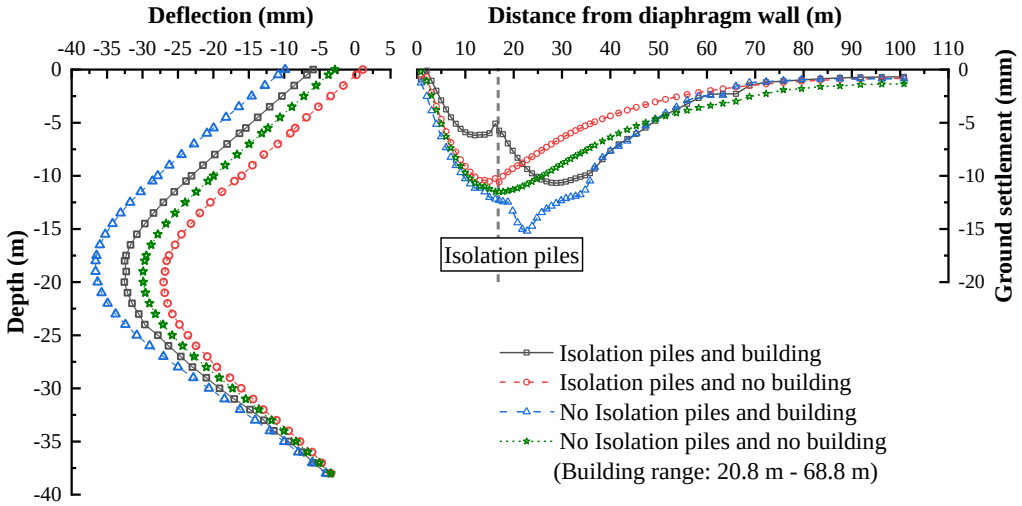

Fig. 7 Lateral displacement of diaphragm walls and surface settlement after excavation

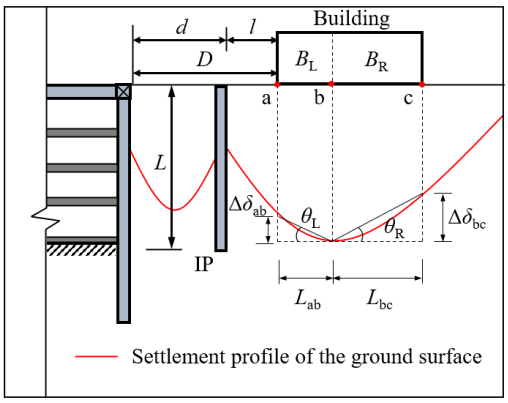

Fig. 10 Parameter diagram

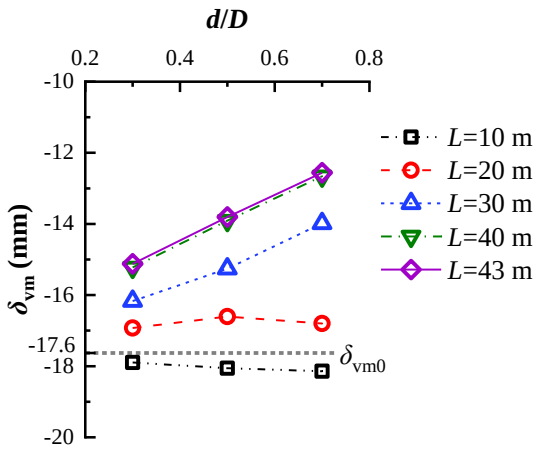

Fig. 11 Maximum building settlement in different d/D (δ_{vm} means maximum building settlement with IP; δ_{vm0} means maximum building settlement without IP)

displacement gradually moves down with the excavation, and finally locates near the excavation bottom. Existing building caused the whole excavation to move towards the clearing. Meanwhile, because the bottom of diaphragm walls is not embedded into rock and lead to a poor embedded effect, resulting in a certain lateral displacement. The deviation between the numerical simulation results and the field data is inherent in the numerical software simulation and is considered acceptable.

Fig. 8 shows the comparison between numerical results and field data for surface settlement and building settlement. There are 12 measuring points for building settlement, but 4 of which were damaged during the construction process. And the middle line of the measuring points of surface settlement was chosen into comparison. It can be seen from Fig. 8 that the simulation results are in good agreement with the filed data. The isolation piles can significantly decrease the surface settlement, especially in the area around the piles, making the settlement curve present a “double groove” characteristic.

4.2 Supporting effect of isolation piles

The accuracy of numerical modeling and parameter selection is verified by comparison with the field data, and can be used for further analysis. Fig. 9 reflects the lateral displacement of diaphragm walls and surface settlement with or without isolation piles and buildings (corresponding to simulation groups 1-4).

By comparing the lateral displacement of the diaphragm walls, it is found that the top of the diaphragm walls will move towards the excavation due to the asymmetric load caused by existing buildings (Liu *et al.* 2019). Through comparison of different working conditions, it is found that the adjacent buildings will increase the settlement due to excavation, and the isolation pile can effectively decrease the settlement around the piles. Besides, the surface settlement curve is changed from “groove” type to “double groove” type by isolation piles, indicating that the isolation piles can effectively decrease the additional settlement caused by existing buildings.

4.3 Different positions and lengths of the isolation piles

Schuster *et al.* (2009) illustrated that vertical deformation, horizontal deformation and rotation of the existing buildings can be used as assessments of excavation-induced building damage. And for buildings with low storeys, horizontal deformation plays an unimportant role on building safety. Therefore, only vertical deformation δ_v and building rotation θ were considered in the analysis.

The parameters which will be used are shown in Fig. 10, where D represents the distance between the building and the excavation, d represents the distance between the isolation piles and the excavation, l represents the distance between the isolation piles and the building, L represents the length of the piles, IP means the isolation piles, a and c are the position of the building edge, b is the position of the maximum settlement point, B_L is the part of the building between a and b, B_R is the part of the building between b and c, $\Delta\delta_{ab}$ is the differential settlement between a and b, $\Delta\delta_{bc}$ is the differential settlement between b and c, L_{ab} is the distance between a and b, L_{bc} is the distance between b and c, θ_L and θ_R are the building rotation of the left part of the building and the right part of the building, respectively (clockwise rotation is positive), θ_L and θ_R can be calculated by formula (8) and (9) respectively.

$$\theta_L = \frac{\Delta\delta_{ab}}{L_{ab}} \tag{8}$$

$$\theta_R = \frac{\Delta\delta_{bc}}{L_{bc}} \tag{9}$$

In order to obtain the general law about the influence of the isolation piles, it is assumed that the width of the building is 20 m, and the distance of the isolation piles was considered using the relative position d/D. Two situations with different building locations, D=10 m and D=20 m, were analyzed to study the influence of the isolation piles.

4.3.1 D=10 m

In this part, the building was assumed at 10 m near the excavation, and the isolation piles were set at d/D=0.3, 0.5

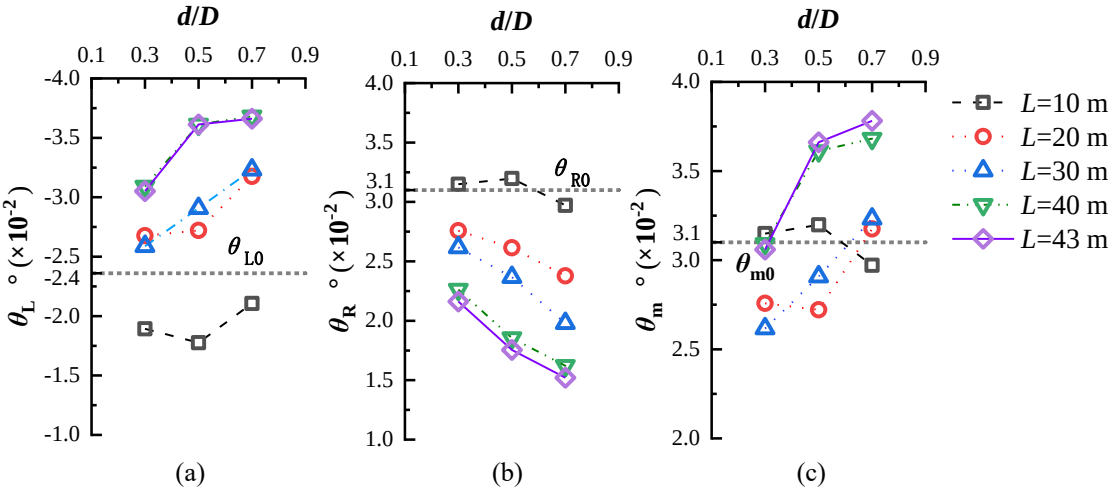

Fig. 12 Building rotation at different positions of the isolation piles (θ_{L0} means building rotation of B_L without IP; θ_{R0} means building rotation of B_R without IP; θ_{m0} means maximum building rotation without IP)

and 0.7, respectively. The lengths of the piles were valued as 10 m, 20 m, 30 m, 40 m and 43 m, respectively, in which 20 m is about the real length and 43 m is embedded into the rock. The specific simulation conditions can be seen in groups 6-20 in Table 6. The maximum settlement δ_{vm} under different position and length of the isolation piles are shown in Fig. 11.

By comparing the maximum building settlement with isolation piles δ_{vm} with those without isolation piles δ_{vm0}, it is found that when L=10 m, δ_{vm} is greater than δ_{vm0} (-17.6 mm), indicating a negative effect on controlling building settlement. It is mainly caused by the following two aspects. On the one hand, the construction of the isolation piles will disturb the surrounding soil and lead to settlement before excavating. On the other hand, if the pile length is too short, the settlement along the piles may be larger than surrounding soils, which will pull the soils down owing to the downward friction (Jiang *et al.* 2008, Haigh and Madabhushi 2011). When L≥20 m, isolation piles can effectively reduce δ_v, and the supporting effect will increase with the increase of d/D.

In most of the engineering case on building deformation, the change of building rotation θ may have a greater impact on building safety (Maddah and Soroush 2020, Piciullo 2021). Fig. 12 shows the variation of θ at different positions of the isolation piles, where θ_L is shown in Fig. 12(a), θ_R is shown in Fig. 12(b) (the meaning of θ_L and θ_R can be seen in Fig. 10), and θ_m is the maximum building rotation, which can be calculated by formula (10), and as is shown in Fig. 12(c).

$$\theta_m = \max\{|\theta_L|, |\theta_R|\} \tag{10}$$

Fig. 12(a) shows that in general, θ_L will increase with the increase of d/D and L. Only when L=10 m, θ_L is less than θ_{L0}, while in other situations, θ_L is larger than θ_{L0}, indicating that in most of the situation, isolation piles will increase building rotation θ. Fig. 12(b) shows that when L≥20 m, θ_R is less than θ_{R0}, and θ_R will decrease with the increase of d/D and L. The reason is that the distance between the building and the excavation is so small that the

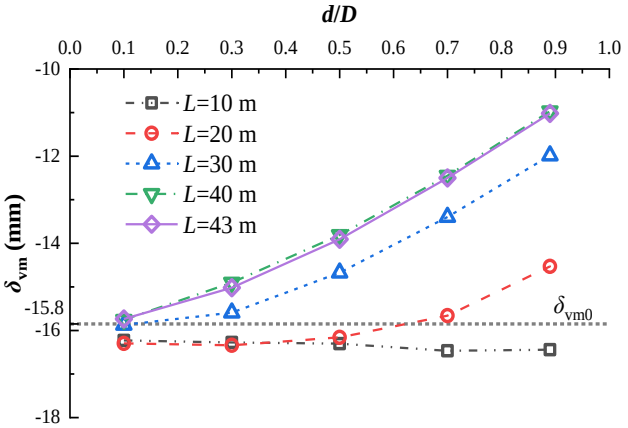

Fig. 13 Maximum building settlement in different d/D (δ_{vm} means maximum building settlement with IP; δ_{vm0} means maximum building settlement without IP)

location of the maximum settlement is within the building range, which will lead to the left part of the building dumping outside and the right part of the building dumping inside. In this situation, the isolation piles will enlarge these trends owing to its effect of controlling the settlement. The problem will be further analyzed in section 4.5. Fig. 12(c) reveals that the isolation piles have little effect on θ_m when L=10 m. But when L≥20 m, θ_m will increase with the increase of d/D and L, indicating that when d/D and L are large enough, the isolation piles will lead to the trend of θ_m>θ_{m0} and present a negative effect on building safety. When d/D and L are not so large, θ_m may smaller than θ_{m0}, indicating that the isolation piles can control the building rotation θ to a certain extent. In summary, for buildings location D=10 m, blindly increasing pile length L and reducing d/D may have a opposite effect on controlling the building deformation.

4.3.2 D=20 m

Similarly, the building was assumed at 20 m near the excavation, and the isolation piles were set at d/D=0.1, 0.3, 0.5 0.7 and 0.9, respectively. The lengths of the piles were

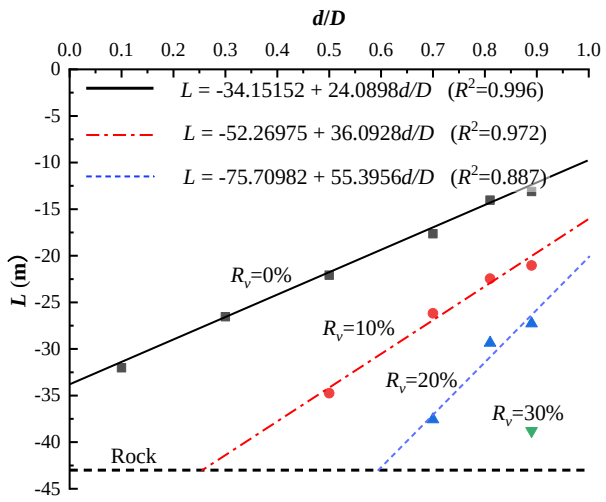

Fig. 14 R_v in different d/D and L

valued as 10 m, 20 m, 30 m, 40 m and 43 m, respectively, in which 20 m is about the real length and 43 m is embedded into the rock. The specific simulation conditions can be seen in groups 22-46 in Table 6.

The maximum settlement δ_{vm} under the action of isolation piles with different lengths L are shown in Fig. 13. It is found that δ_{vm} is greater than δ_{vm0} when L=10 m and when L= 20 m, d/D=0.1, 0.3, 0.5, indicating that the isolation piles will play a negative role in controlling building settlement in these cases. In other cases, δ_m is less than δ_{vm0}, which means isolation piles are helpful in controlling building settlement. In general, the supporting effect of isolation piles on controlling building settlement is enhanced with the increase of d/D and L.

In order to evaluate the supporting effect of isolation piles on controlling building settlement, the control efficiency is defined as R_v, which is calculated by formula (11).

$$R_v = \frac{\delta_{vm} - \delta_{vm0}}{\delta_{vm0}} \tag{11}$$

where δ_{vm} is the maximum building settlement with isolation piles, and δ_{vm0} is the maximum building settlement without isolation piles.

The control efficiency R_v for isolation piles of different positions and lengths on the maximum building settlement is shown in Fig. 14. R_v=0 means isolation piles has no influence on the building deformation caused by excavation, the curve of R_v=0 shows a trend for approximately linear decreasing appropriate length(L) of isolation piles with increasing of the relative position between isolation piles and building d/D. It can be seen that in order to achieve the same value of R_v, the pile length L is linearly correlated with d/D. When d/D is constant, R_v will significantly increase with the increase of L, and when L is constant, R_v will significantly increase with the increase of d/D. When the pile bottom is above R_v=0 %, the isolation piles will have negative effect on the control of building settlement. When the pile bottom is below R_V=0 %, the isolation pile has a positive control effect on the building settlement.

Fig. 15 shows the change of building rotation θ under the action of isolation piles when D=20 m. It can be found that the isolation piles have a significant effect on controlling building rotation θ. The change of θ_L is shown

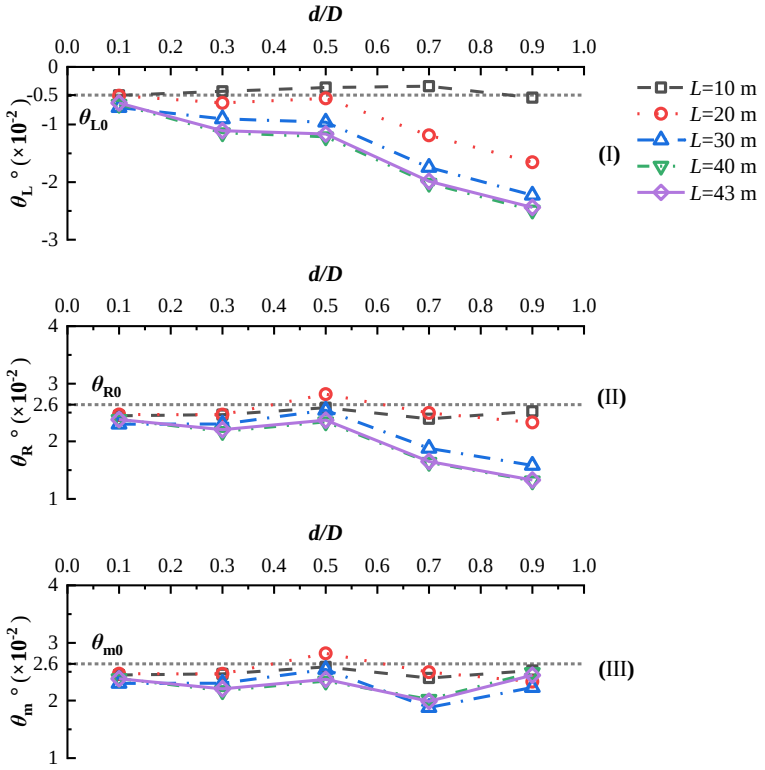

Fig. 15 Building rotation in different d/D (θ_{L0}, θ_{R0} and θ_{m0} is building rotation without IP)

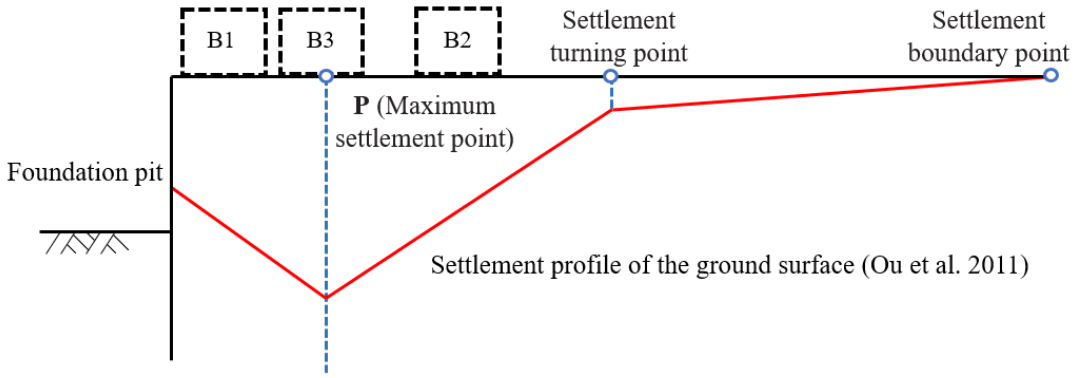

Fig. 16 The relationship between building locations and the maximum settlement point P

in Fig. 15(I), and the change of θ_R is shown in Fig. 15(II) (the meaning of θ_L and θ_R can be seen in Fig. 10), Fig. 15 (III) indicates the change of the maximum building deformation θ_m.

Results in Fig. 15(I) show that θ_L will increase with d/D and L increase, and θ_L is less than θ_{L0} only when L=10 m. When $L\geq$10 m, θ_L is greater than θ_{R0}, indicating that the isolation piles will increase the building rotation of the left part of the building. Results in Fig. 15(II) reveal that θ_R is greater than θ_{R0} only when L=20 m and d/D=0.5, and in other cases, θ_R is always less than θ_{R0}. Besides, θ_R will decrease with d/D and L increase. It can be concluded that for the right part of the building, isolation piles can effectively decrease the building rotation.

Fig. 15(III) shows that the optimal position of the isolation piles for controlling effect on the building rotation θ_m is d/D=0.7. Overlarge value of d/D will decrease the supporting effect because that the isolation piles which are too close to buildings will observably increases the settlement difference of the left part of the buildings and lead to large rotation.

4.4 Different building positions

Ou *et al*. (2011) proposed the characteristic curve of surface settlement outside the diaphragm walls due to excavations, as is shown in Fig. 16. The building positions were divided into three cases based on the settlement curve: B1, B2 and B3. B1 is located within the range of the point P (point P is the location of the maximum settlement without building and isolation piles and in this paper, it equals 16.2 m). B2 is located outside the point P, and B3 is near the point P. To protect the adjacent buildings, a certain space is usually reserved between buildings and excavations in actual projects, leading to the exceeding of the building edge to the point P. Thus, only B2 and B3 are considered in this section.

In the above section, it was found that though too short isolation piles have poor supporting effect on controlling building deformation, too long isolation piles does not always mean better supporting effect, but causes the waste of materials. Therefore, in this section, it is assumed that the pile length is 30 m, the width of the building is 20 m, and the building is located in different positions outside the pit

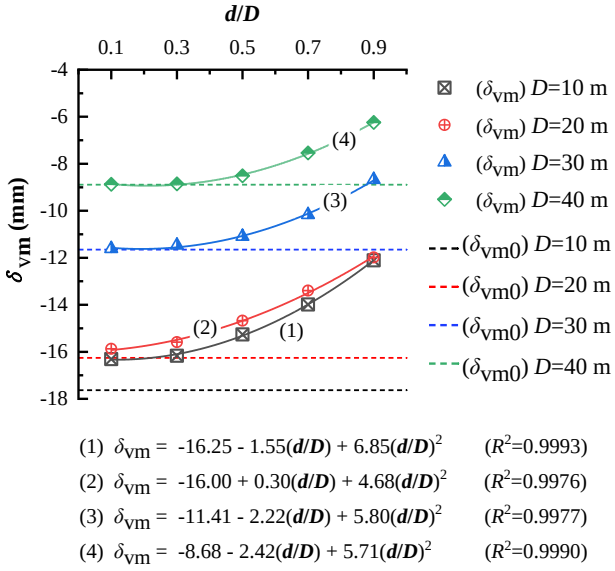

Fig. 16 Maximum building settlement δ_m in different locations of building and isolation pile (pile length L=30 m)

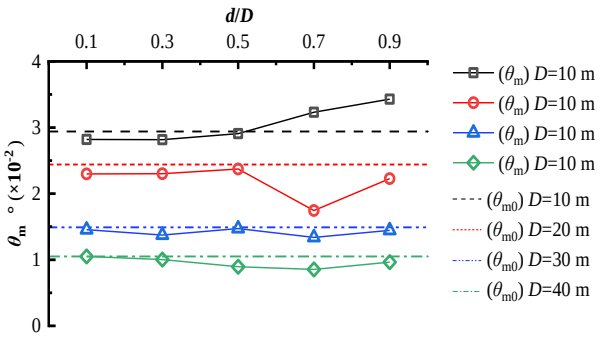

Fig. 17 θ_m in different locations of building and d/D when L=30 m

to study the influence of the relative building position on the supporting effect of the isolation piles (D=10 m, 20 m, 30 m, 40 m), where D=10 m corresponds to B3, and D=20 m, 30 m, 40 m corresponds to B2. The specific simulation conditions can be seen in groups 5, 8, 13, 18, 21, 24, 29, 34, 39, 44, 47-56 in Table 6.

The influence of the building position D and the relative position between the isolation piles and building d/D on the

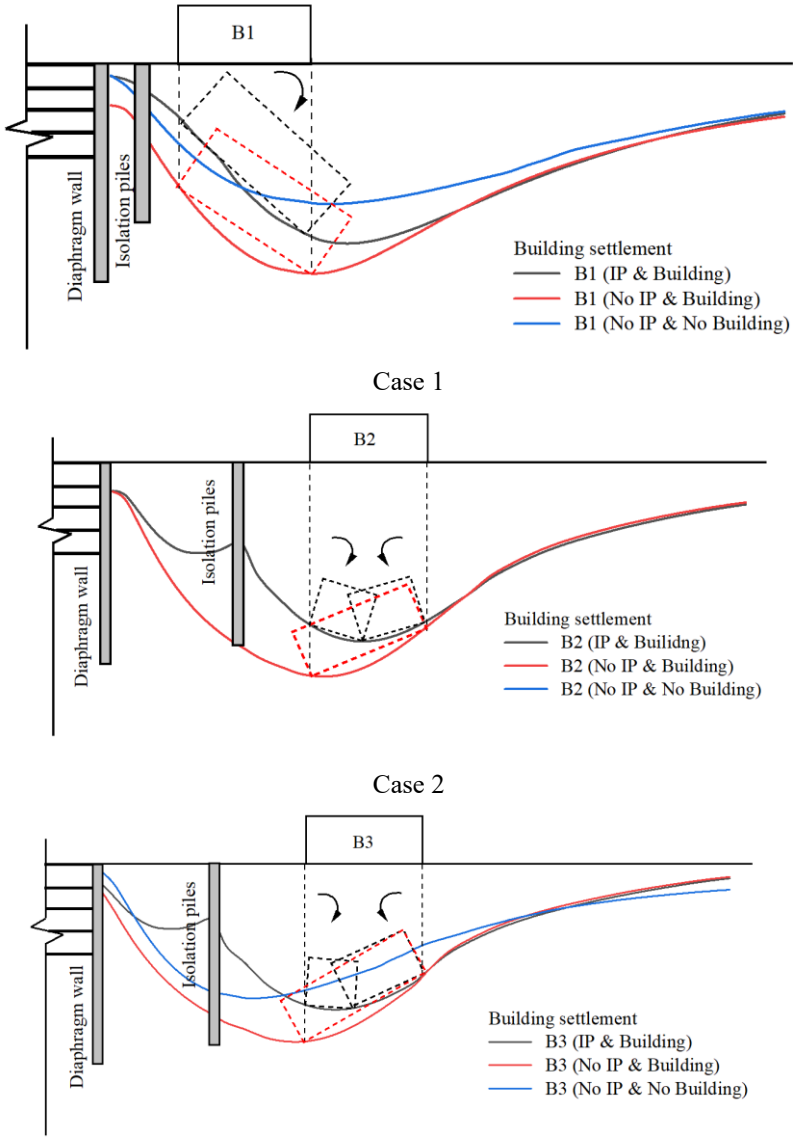

Fig. 18 Characteristics of building deformation of B1, B2 and B3. (IP means isolation piles)

maximum building settlement δ_{vm} is shown in Fig. 17. It reveals that the maximum building settlement with isolation piles δ_{vm} is obviously smaller than the maximum settlement without isolation piles δ_{m0}, indicating that the isolation piles can effectively control δ_{vm} of buildings at different positions. δ_{vm} shows a quadratic function relationship with d/D, and the supporting effect is enhanced with the increase of d/D. When the building is far away from the excavation (D=30 m and 40 m) and $d/D \leq 0.5$, isolation piles have little effect on controlling building settlement. On the contrary, isolation piles have a certain effect on controlling building settlement in the condition of $d/D \geq 0.5$. However, for buildings closer to the excavation (D=10 m and 20 m), isolation piles will have a better effect in controlling building settlement. In summary, the supporting effect of isolation piles on buildings near the excavation is significantly better than that of buildings far from the excavation.

The influence of the building location D and the relative position between the isolation piles and building d/D on the maximum building rotation θ_m is shown in Fig. 18. It is shown that the isolation piles can decrease the maximum building rotation θ_m to a certain extent when $d/D \leq 0.5$, but the influence is not obvious. In the condition of $d/D \geq 0.5$ and D=10 m, the maximum building rotation with isolation piles θ_m is greater than those without isolation piles, indicating that the isolation piles have a negative effect on controlling θ_m. The isolation piles will get the best supporting effect when D=20 m, and the supporting effect is not obvious when D=30 m or 40 m. In summary, for buildings of D=20 m, 30 m and 40 m, the isolation piles will achieve the best supporting effect of controlling the maximum building rotation θ_m in the condition of d/D=0.7, and the control efficiency is 28.64 %, 10.17 % and 9.89 %, respectively.

4.5 Adaptability analysis of isolation piles

Combined with the above research about the supporting effect of isolation piles on different building positions, it can be concluded into three cases and were shown in Fig. 19.

Case 1: When a building is located within the range of the maximum settlement point P (in Fig. 16), the surface settlement curve under the action of isolation piles presents a 'groove' type. The isolation piles can effectively reduce the building settlement δ_v but increase building rotation θ. Besides, θ will increase with the increase of d/D (the relative position between isolation piles and buildings) and L (pile length). Therefore, in this case, the isolation piles may have poor control effect.

Case 2: When a building is located outside the point P, the surface settlement curve under the action of isolation piles presents a 'double groove' type. In this case, the isolation piles with sufficient length L can effectively decrease δ_v and θ. The effect of controlling θ is not remarkable when d/D is small, but when d/D is large, it will significantly affect the building rotation, and θ will first decrease and then increase with the increase of d/D. The optimum position of the isolation piles is the relative position d/D=0.7. In general, in this case, reasonable construction of isolation piles can achieve an optimum supporting effect.

Case 3: When a building is located near the point P, the surface settlement curve under the action of isolation piles presents a 'double groove' type. The sufficient long isolation piles can effectively decrease δ_v, but the supporting effect of controlling θ is more complicated. In this case, θ is closely related to d/D and L. Reasonable design of isolation piles can effectively control θ, otherwise, it will have the opposite effect.

5. Conclusions

Based on the deep excavation of Hongqiao Subway Station in Nanjing, China, a series of numerical simulation model were established and analyzed to study the supporting effect of the isolation piles. Building settlement δ_v and building rotation θ were took as the measurement indexes of building damage and pile positions d/D, pile lengths L and building positions D were took as the influence factors. The main results are summarized as follows:

- Adjacent buildings will increase surface settlement and the deformation of the diaphragm walls, while the existence of isolation piles can effectively control these. The surface settlement curve will change from “groove” type to “double groove” type under the action of the isolation piles.
- Sufficient long isolation piles can effectively control building settlement δ_v, and increase of pile length L and relative position of piles d/D can significantly improve the control efficiency R_v. However, when L is small, the isolation piles will have a negative effect on controlling δ_v, leading to increase of δ_v.
- When an existing building is within the range of the maximum settlement point P (in Fig. 16), the maximum building rotation with isolation piles θ_m will increase with the increase of L and d/D, or even exceed the maximum building rotation without isolation piles θ_{m0}, leading to negative effects. When a building is located outside the point P, the isolation piles can achieve positive effect on controlling θ, and the optimum position is d/D=0.7.
- In terms of controlling building settlement δ_v, the supporting effect of isolation piles on the buildings close to the excavation is obviously better than those far away from the excavation. In terms of controlling building rotation θ, the isolation piles have a better effect on the buildings located outside the point P and near the excavation, while the buildings located within the point P may lead to increase of θ under the action of isolation piles.

Acknowledgements

The research described in this paper was financially supported by the National Natural Science Foundation for Young Scientists of China (Grant No. 52104076) and Graduate Scientific Research and Innovation Foundation of Chongqing, China (Grant No. CYB20031).

References

Bilotta, E. (2008), “Use of diaphragm walls to mitigate ground movements induced by tunnelling”, *Geotechnique*, **58**(2), 143-155. https://doi.org/10.1680/geot.2008.58.2.143.

Bilotta, E. and Russo, G. (2011), “Use of a line of piles to prevent damages induced by tunnel excavation”, *J. Geotech. Geoenviron. Eng.*, **137**(3), 254-262. https://doi.org/10.1061/(ASCE)GT.1943-5606.0000426.

Canakci, H. and Hamed, M. (2017), “Experimental study on axial response of different pile materials in organic soil”, *Geomech. Eng.*, **12**(6), 899-917. https://doi.org/10.12989/gae.2017.12.6.899.

Castaldo, P., Calvello, M. and Palazzo, B. (2013). “Probabilistic analysis of excavation-induced damages to existing structures”, *Comput. Geotech.*, **53**, 17-30. https://doi.org/10.1016/j.compgeo.2013.04.008.

Chen, J.J., Zhu, Y.F., Li, M.G. and Wen, S.L. (2015), “Novel excavation and construction method of an underground highway tunnel above operating metro tunnels”, *J. Aerosp. Eng.*, **28**(6), A4014003. https://doi.org/10.1061/(ASCE)AS.1943-5525.0000437.

Chen, R.P., Meng, F.Y., Li, Z.C., Ye, Y.H. and Ye, J.N. (2016), “Investigation of response of metro tunnels due to adjacent large excavation and protective measures in soft soils”, *Tunnel. Undergr. Space Technol.*, **58**, 224-235. https://doi.org/10.1016/j.tust.2016.06.002.

Chowdhury, S.S., Deb, K. and Sengupta, A. (2013), “Estimation of design parameters for braced excavation: Numerical study”, *Int. J. Geomech.*, **13**(3), 234-247. https://doi.org/10.1061/(ASCE)GM.1943-5622.0000207.

Cui, Q.L., Wu, H.N., Shen, S.L., Yin, Z.Y. and Horpibulsuk, S. (2016), “Protection of neighbor buildings due to construction of shield tunnel in mixed ground with sand over weathered granite”, *Environ. Earth Sci.*, **75**(6), 1-11. https://doi.org/10.1007/s12665-016-5300-7.

Demeijer, O., Chen, J.J., Li, M.G., Wang, J.H. and Xu, C.J. (2018),

"Influence of passively loaded piles on excavation-induced diaphragm wall displacements and ground settlements", *Int. J. Geomech.*, **18**(6), 04018052. https://doi.org/10.1061/(ASCE)GM.1943-5622.0001126.

Gao, G.Y., Li, Z.Y., Qiu, C. and Yue, Z.Q. (2006), "Three-dimensional analysis of rows of piles as passive barriers for ground vibration isolation", *Soil Dyn. Earthq. Eng.*, **26**(11), 1015-1027. https://doi.org/10.1016/j.soildyn.2006.02.005.

Haigh, S.K. and Madabhushi, S.P.G. (2011), "Centrifuge modelling of pile-soil interaction in liquefiable slopes", *Geomech. Eng.*, **3**(1), 1-16. https://doi.org/10.12989/gae.2011.3.1.001.

Jiang, J., Qi, B. and Liu, G.B. (2008), "Factors and prediction on deformation of soldier piles in deep foundation pits in soft area", *Chin. J. Geotech. Eng.*, **30**(S1), 363-368. (in Chinese)

Jiang, S.Y., Du, C.B. and Sun, L.G. (2018), "Numerical analysis of sheet pile wall structure considering soil-structure interaction", *Geomech. Eng.*, **16**(3), 309-320. https://doi.org/10.12989/gae.2018.16.3.309.

Kumara, J.J., Kurashina, T. and Kikuchi, Y. (2016), "Effects of pile geometry on bearing capacity of open-ended piles driven into sands", *Geomech. Eng.*, **11**(3), 385-400. https://doi.org/10.12989/gae.2016.11.3.385.

Li, M.G., Chen, J.J., Xu, A.J., Xia, X.H. and Wang, J.H. (2014), "Case study of innovative top-down construction method with channel-type excavation", *J. Constr. Eng. Manage.*, **140**(5), 05014003. https://doi.org/10.1061/(ASCE)CO.1943-7862.0000828.

Liu, S.H., Yang, J.S., Fu, J.Y. and Zheng, X.C. (2019), "Performance of a deep excavation irregular supporting structure subjected to asymmetric loading", *Int. J. Geomech.*, **19**(7), 05019007. https://doi.org/10.1061/(ASCE)GM.1943-5622.0001468.

Maddah, A. and Soroush, A. (2020), "A comprehensive numerical study on building-excavation", *Civil Eng. J.-Tehran*, **6**(2), 326-343. https://doi.org/10.28991/cej-2020-03091474.

Maddah, A., Soroush, A. and Shafipour, R. (2021), "A new concept for interpretation of building-excavation interaction in 3D conditions", *Tunnel. Undergr. Space Technol.*, **109**, 103757. https://doi.org/10.1016/j.tust.2020.103757.

Mansouri, H. and Asghari-Kaljahi, E. (2019), "Two dimensional finite element modeling of Tabriz metro underground station L2-S17 in the marly layers", *Geomech. Eng.*, **19**(4), 315-327. https://doi.org/10.12989/gae.2019.19.4.315.

Mitew-Czajewska, M. (2018), "A study of displacements of structures in the vicinity of deep excavation", *Arch. Civil Mech. Eng.*, **19**(2), 547-556. https://doi.org/10.1016/j.acme.2018.11.010.

Nikiforova, N.S. and Vnukov, D.A. (2012) "Geotechnical cut-off diaphragms for built-up area protection in urban underground development", *7th International Symposium on Geotechnical Aspects of Underground Construction in Soft Ground*, Rome, Italy, May.

Ou, C.Y. and Hsieh, P.G. (2011), "A simplified method for predicting ground settlement profiles induced by excavation in soft clay", *Comput. Geotech.*, **38**(8), 987-997. https://doi.org/10.1016/j.compgeo.2011.06.008.

Ou, C.Y., Teng, F.C. and Wang, I.W. (2008), "Analysis and design of partial ground improvement in deep excavations", *Comput. Geotech.*, **35**(4), 576-584. https://doi.org/10.1016/j.compgeo.2007.09.005.

Piciullo, L., Ritter, S., Lysdahl, A.O.K., Langford, J. and Nadim, F. (2021), "Assessment of building damage due to excavation-induced displacements: The GIBV method", *Tunnel. Undergr. Space Technol.*, **108**, 103673. https://doi.org/10.1016/j.tust.2020.103673.

Qian, J.G., Tong, Y.M., Mu, L.L., Lu, Q. and Zhao, H.Q. (2020), "A displacement controlled method for evaluating ground settlement induced by excavation in clay", *Geomech. Eng.*, **20**(4), 275-285. https://doi.org/10.12989/gae.2020.20.4.275.

Rezvani, R. and Tutunchian, M.A. (2021). "Horizontal displacement of urban deep excavated walls supported by multistrands anchors, steel piles, and in situ concrete piles: Case study", *Int. J. Geomech.*, **21**(1), 05020008. https://doi.org/10.1061/(ASCE)GM.1943-5622.0001890.

Schuster, M., Kung, G.T.C., Juang, C.H. and Hashash, Y.M.A. (2009), "Simplified model for evaluating damage potential of buildings adjacent to a braced excavation", *J. Geotech. Geoenviron. Eng.*, **135**(12), 1823-1835. https://doi.org/10.1061/(ASCE)GT.1943-5606.0000161.

Shen, Y.J., Wu, Z.J., Xiang, Z.L. and Yang, M. (2017), "Physical test study on double-row long-short composite anti-sliding piles", *Geomech. Eng.*, **13**(4), 621-640. https://doi.org/10.12989/gae.2017.13.4.621.

Son, M. and Cording, E.J. (2005), "Estimation of building damage due to excavation-induced ground movements", *J. Geotech. Geoenviron. Eng.*, **131**(2), 162-177. https://doi.org/10.1061/(ASCE)1090-0241(2005)131:2(162).

Talha, S.B. (2001), "Deformation behaviors of a retaining wall for a deep basement excavation with semi-top down method", *Proceedings of the 14th Southeast Asian Geotechnical Conference*, Hong Kong, China, December.

Tan, Y., Huang, R.Q., Kang, Z.J. and Bin, W. (2016), "Covered semi-top-down excavation of subway station surrounded by closely spaced buildings in downtown Shanghai: Building response", *J. Perform. Constr. Facil.*, **30**(6), 1-26. https://doi.org/10.1061/(ASCE)CF.1943-5509.0000892.

Wang, J.H., Xu, Z.H. and Wang, W.D. (2010), "Wall and ground movements due to deep excavations in shanghai soft soils", *J. Geotech. Geoenviron. Eng.*, **136**(7), 985-994. https://doi.org/10.1061/(ASCE)GT.1943-5606.0000299.

Yang, X.H., Jia, M.C. and Ye, J.Z. (2020), "Method for estimating wall deflection of narrow excavations in clay", *Comput. Geotech.*, **117**, 103224. https://doi.org/10.1016/j.compgeo.2019.103224.

Yao, A.J., Yang, X.J. and Dong, L. (2012), "Numerical analysis of the influence of isolation piles in metro tunnel construction of adjacent buildings", *International Conference on Structural Computation and Geotechnical Mechanics*, Kunming, China, March.

Yu, Y., Sun, H.Y. and Juang, C.H. (2018), "A new model for response of laterally loaded piles in soil-rock mixtures", *Comput. Geotech.*, **104**, 237-246. https://doi.org/10.1016/j.compgeo.2018.08.021.

Orazalin, Z.Y., Whittle, A.J. and Olsen, M.B. (2015), "Three-dimensional analyses of excavation support system for the Stata Center basement on the MIT campus", *J. Geotech. Geoenviron. Eng.*, **141**(7), 1-14. https://doi.org/10.1061/(ASCE)GT.1943-5606.0001326.

Zhang, W.G., Li, Y.Q., Goh, A.T.C. and Zhang, R.H. (2020), "Numerical study of the performance of jet grout piles for braced excavations in soft clay", *Comput. Geotech.*, **124**, 103631. https://doi.org/10.1016/j.compgeo.2020.103631.

Zheng, G., Wang, F.J., Du, Y.M., Diao, Y., Lei, Y.W. and Cheng, X.S. (2018), "The efficiency of the ability of isolation piles to control the deformation of tunnels adjacent to excavations", *Int. J. Civil Eng.*, **16**(10B), 1475-1490. https://doi.org/10.1007/s40999-018-0335-7.

CC